Limnology and Oceanography
FLUIDS & ENVIRONMENTS

ORIGINAL ARTICLE

Rotational diffusion of particles in turbulence

Colin R. Meyer, Margaret L. Byron, and Evan A. Variano

Abstract

Through laboratory measurements, we compared the rotation of spherical and ellipsoidal particles in homogeneous, isotropic turbulence. We found that the particles' angular velocity statistics are well described by an Ornstein–Uhlenbeck (OU) process. This theoretical model predicts that the Lagrangian autocovariance of particles' angular velocity will decay exponentially. We measured the autocovariance by using stereoscopic particle image velocimetry (SPIV) applied to spherical and ellipsoidal particles whose size was within the inertial subrange of the ambient turbulence. SPIV resolves the motion of points interior to the particles, from which we calculated the solid body rotation of the particles. This provided us with the angular velocity time series for individual particles. Through ensemble statistics, we determined the autocovariance of angular velocity and confirmed that it matches the form predicted by an OU process. We found that in this stochastic framework the autocovariances of both the ellipsoids and spheres are statistically identical, suggesting that rotation is controlled by the large scales of turbulence. We can further use the autocovariance curve to quantify the turbulent rotational diffusivity and discuss its implications for the transport of aquatic organisms in natural turbulence.

Keywords: particle-laden flows, homogeneous turbulence, isotropic turbulence, multiphase flows, biological fluid dynamics

Introduction

[1] Rotation is a fundamental characteristic of the kinematics of ecologically relevant particles, notably plankton and aggregates (e.g., marine snow). Rotation impacts the behavior of individual particles through its effects on drag (Clift et al. 2005; Mortensen et al. 2008b), as well as navigation and perception. For example, rotation may interfere with gravitaxis and directed swimming of plankton (Machemer and Bräucker 1992; Roberts and Deacon 2002). Two-particle interactions, such as collision and avoidance, are dependent on rotation and orientation (Koch and Shaqfeh 1989). Rotation may also interfere with the mechanoperception of prey by copepods and larvae, in some cases preventing prey capture (Yamazaki and Squires 1996; Visser 2001). The behavior of entire particle communities may also be affected by rotation, for example, by controlling preferential alignment. Particle alignment can be due to settling or shear (Roberts and Deacon 2002; Reidenbach et al. 2009); rotational diffusion acts as a competing mechanism that works against alignment. The interplay among these mechanisms can cause unique visual signatures as the alignment evolves, due to alignment's effects on the optical properties of a suspension. Because plankton and aggregates are typically nonspherical, it is necessary to consider the effect of shape on their rotation. This study compares rotational dynamics of spherical and nonspherical particles suspended in a turbulent flow.

Department of Civil and Environmental Engineering, University of California, Berkeley, California 94720, USA

Correspondence to Colin R. Meyer, colinrmeyer@gmail.com

Limnology and Oceanography: Fluids and Environments • 3 (2013): 89–102 • DOI 10.1215/21573689-2326592

[2] For both spherical and nonspherical particles, rotation significantly affects the wake structure behind a particle and thus the forces coupling the particle and surrounding fluid (Batchelor 1967; Giacobello et al. 2009). These forces, in turn, set the particle rotation rate by causing angular acceleration (Bagchi and Balachandar 2002; Shin and Koch 2005). This feedback can lead to complex behaviors, including broken symmetry in quiescent fluid (Jenny et al. 2004), rotation in a direction opposite to local vorticity during the transient approach to equilibrium in a steady shear flow (Bagchi and Balachandar 2002), and spherical particles that do not rotate at half the local fluid vorticity in turbulent flow (Mortensen et al. 2007, 2008a). Recent work by Bellani et al. (2012) has shown that the addition of spherical and ellipsoidal particles into homogeneous turbulence changes the spectral slope of the fluid-phase turbulence. Furthermore, Eulerian rotation statistics of the spherical and ellipsoidal particles are quite different from the fluid enstrophy (Bellani et al. 2012).

[3] Complex feedbacks between particles and turbulence become particularly interesting when particles are larger than the local minimum scale of shear, for example, the Kolmogorov length scale. In such cases, the particle experiences nonlinear shear and directly influences the turbulent field simply by taking up space. Aquatic organisms that are typically within this size range are the nektoplankton—organisms with intermittent control over their direction and orientation, such as fish larvae. Such animals, having length scales within the inertial subrange of ambient turbulence, are subjected to eddies both larger and smaller than themselves. Many organisms at this size scale have evolved physical adaptations (as manifested in fin and body shape) to better control and stabilize their position in the flow (Webb and Cotel 2010). Local rotation (about the body axes of the animal; i.e., yaw, pitch, and roll) is important for navigation and stabilization. However, global rotation matters as well. For example, Tritico and Cotel (2010) showed that loss of postural control is greatly increased when fish swim through horizontally oriented eddies compared with vertically oriented eddies. Excessive rotation can also disorient organisms with respect to gravity, subjecting them to increased predation (Čada 1997).

[4] Key questions for predicting particle motions are how turbulence and particle shape interact to set the magnitude of particle rotation, and how long an angular velocity value tends to persist. This value will be determined by the interaction of a particle with the turbulent flow, and for large particles the interaction cannot be calculated with Stokes's or Jefferey's (1922) formulas. This "persistence" or "correlation" timescale of particle angular velocities is an important input when modeling particle motion as a stochastic process (Naso and Prosperetti 2010). This can be useful when specifying a stochastic drag model (Rybalko et al. 2012). It can also be used when studying particle orientation dynamics (e.g., Durham et al. 2009).

[5] The stochastic description of particle rotation may take any number of forms, but the most convenient is a diffusion process. This is the commonly used paradigm in mass transport, and Eulerian models for scalar diffusion in shear flows have been studied extensively (Richardson 1926; Taylor 1953). Many environmental transport processes can be modeled as random walks, and stochastic processes are a formal method for working with random walks (Fischer et al. 1979). Of specific interest here is the Ornstein–Uhlenbeck (OU) process, a stochastic process that describes diffusion (Doob 1942). Along with its corresponding stochastic differential equation (the Langevin equation), the OU process can be an effective model of diffusive mass transport in turbulence (Pope 2000).

[6] In this study we examined the hypothesis that the OU process can describe the angular velocity of spherical and ellipsoidal particles in turbulent flow. This approach allows the time-dependent evolution of a particle's orientation to be described as a random walk in orientation space, as a function of the angular velocity statistics. Rotational diffusion is analogous to translational diffusion, which describes the evolution of a particle's location as a function of turbulent velocity statistics (Berg 1983). We tested this hypothesis by measuring the Lagrangian autocovariance and probability density functions (PDFs) of particles' angular velocity and comparing these with the OU model.

Methods

Analytical Model for Rotation

[7] An OU process is completely characterized by a Gaussian distribution and an exponentially decaying autocovariance, both of which are statistically stationary (Doob 1942). The autocovariance of time series $a(t)$ is defined as $R(\tau) \equiv \langle a(t)a(t+\tau)\rangle$, where t is time, τ is a time lag, and angle brackets denote expectation values. For an OU process, $R(\tau)$ is a negative exponential, that is, $R(\tau) = \sigma^2 e^{-\tau/T}$, where σ^2 is the variance of the distribution of a (which is Gaussian), and the characteristic time T is known as the integral timescale. The OU process has been shown to accurately describe the Lagrangian velocity of fluid parcels in turbulent flow (Pope 2000). One important implication of this is that the OU process can be used to accurately model the turbulent diffusion of a cloud of particles, giving the time-dependent eddy diffusivity, K (Taylor 1922)

$$K(t) = \int_0^t R(\tau)d\tau. \quad (1)$$

This result can be used to apply Fick's law for mass flux in a turbulent flow (Fischer et al. 1979). The time dependence of Eq. 1 is an extremely important feature for biological studies. It allows the diffusion model to be applied at times shorter than the asymptotic limit. Such short-time processes can be crucial in questions of collision and avoidance (Visser and Kiørboe 2006).

[8] We hypothesize that the OU process is also a good model for the rotation of large (i.e., larger than the Kolmogorov scale) particles suspended in a turbulent flow. Specifically, we hypothesized that the Lagrangian time series of angular velocities will follow an OU process. We tested this hypothesis by examining two aspects of the particle rotation statistics. First, we examined whether the PDF of particles' angular velocity is stationary and Gaussian. Second, we examined whether the diagonal components of the Lagrangian angular velocity autocovariance tensor, R_ω, decay exponentially as

$$R_{\Omega_i}(\tau) = \alpha_i^2 e^{-\tau/T_{\Omega_i}}, \quad (2)$$

where T_{Ω_i} is the Lagrangian integral timescale of angular velocity and α_i^2 is the variance of the angular velocity. The autocovariance tensor can be uniquely described by a single index because all of the off-diagonal terms are zero: $R_{\Omega_i}(\tau) = R_{\Omega_i\Omega_i}(\tau)$ (without summation; see Results). Hereafter we refer to Eq. 2 as the autocovariance. The other statistics derived from the autocovariance tensor follow the same convention.

Laboratory Experiment

[9] We examined particle motion in homogeneous, isotropic turbulence generated in a laboratory facility consisting of a symmetrically stirred rectangular turbulence tank driven by a planar forcing element (64 synthetic jets) on each end (Fig. 1). The symmetry contributes to large-scale isotropy, as does the use of two randomly actuated synthetic jet arrays (RASJAs) for the forcing elements (Variano and Cowen 2008). The jets in each RASJA fire in a stochastic pattern that maximizes the shear production of turbulence, similar to an active-grid wind tunnel but without mean flow. The RASJAs allow the tank-scale secondary circulations to be essentially eliminated, which increases the residence time of particles in the test section helping us measure Lagrangian particle trajectories.

[10] The turbulence tank (80 cm vertical by 80 cm lateral by 162 cm axial, where axial is the direction in which the RASJA jets inject momentum) had two screens to prevent particles from interacting with the pumps; these screens defined a central region 80 cm × 80 cm × 75 cm. The flow properties of this tank (without screens) are presented in Bellani et al. (2012) and (with screens) in Bellani and Variano (2012). The fluid-phase turbulence with screens (and without particles) is described in Table 1. The introduction of particles reduces the turbulent kinetic energy, E_k; spheres reduce E_k by 15%, and ellipsoids reduce E_k by 3% (Bellani et al. 2012). These data were obtained from traditional (two-dimensional) particle image velocimetry at the tank center. Isotropy of the flow was evident when comparing the velocity fluctuation magnitudes between the axial and vertical direction. Homogeneity of turbulent statistics was observed in a region surrounding the tank center. Defining the homogeneous region as the region over which velocity statistics (variance, Reynolds stress, integral length scale, Taylor scale, and dissipation rate) do not vary by more than 5%, we found that this region extends beyond ±1 integral length

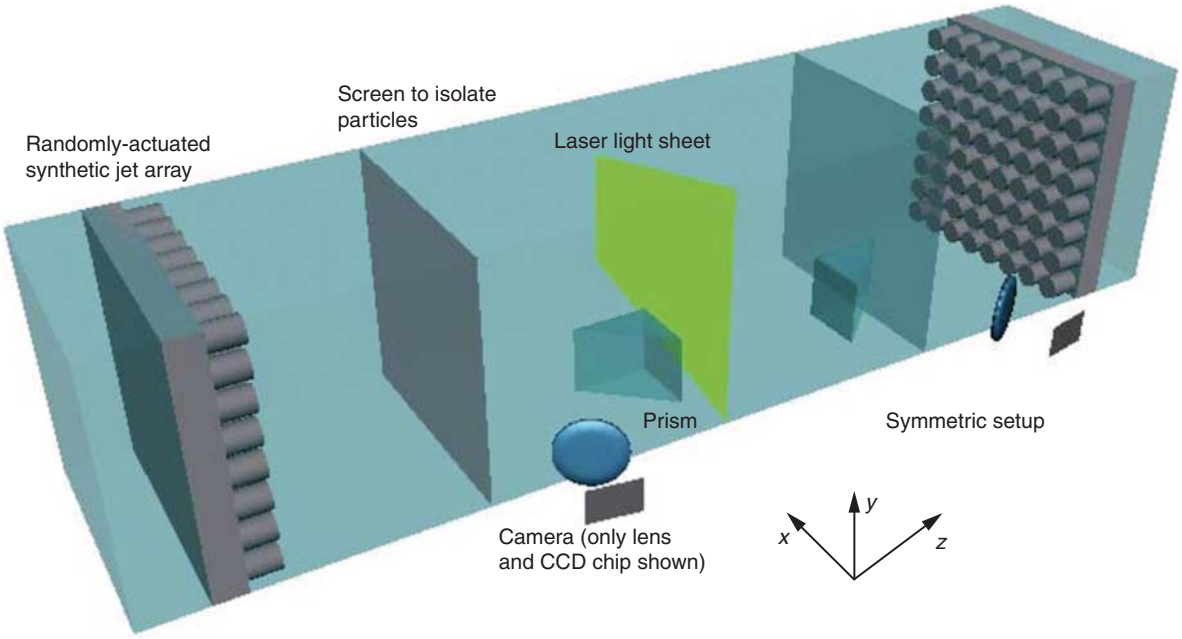

Fig. 1 Schematic of the stirred turbulence tank and stereoscopic imaging. The tank cross section is 80 cm × 80 cm, the screens are separated by 76 cm, and the jet arrays are 180 cm apart. Turbulence is generated by stochastically firing pumps according to the method developed in Variano and Cowen (2008). Axes indicate the laboratory coordinate system, consistent with Bellani et al. (2012).

scale in the axial direction and beyond ±2 integral length scales in the vertical direction. By symmetry, we assumed that the same isotropy and homogeneity observed in the axial and vertical directions would be found in the lateral direction. It is important for the proposed experiments to have a large homogeneous region, because particle rotation statistics are determined by the experiences of a particle over its recent trajectory. By measuring the particle motion at the center of a large homogeneous region, we ensured that the flow experienced by particles during the time shortly before they are measured is a single, well-quantified flow. In other words, the particle statistics we report should not contain a strong signature of flows different from what was determined at the measurement location.

[11] We placed hydrogel spheres (diameter $d = 8\,\text{mm}$) or ellipsoids (major axis $l_e = 16\,\text{mm}$, minor axes $d_e = 8\,\text{mm}$) made of an agarose solution ($4\,\text{g}\,\text{L}^{-1}$)

Table 1 Turbulence statistics of fluid phase without particles in experimental facility, with 95% confidence intervals (CIs). Both λ_z and Λ_x were calculated from the longitudinal autocovariance of fluid-phase velocity. The root mean square velocities (rms) are provided.

Turbulence statistic	Definition (units)	Measurement (95% CI)
Transverse velocity rms	u_{rms} (m s^{-1})	≈0.012 (—)
Vertical velocity rms	v_{rms} (m s^{-1})	0.012 (0.012, 0.012)
Longitudinal velocity rms	w_{rms} (m s^{-1})	0.013 (0.013, 0.013)
Turbulent kinetic energy	$E_k\left(=\frac{1}{2}\left(\sum_1^3 u_{i_{\text{rms}}}^2\right)\right)$ (m^2 s^{-2})	2.3×10^{-4} (2.3×10^{-4}, 2.3×10^{-4})
Taylor microscale	λ_z (m)	8.3×10^{-3} (6.2×10^{-3}, 10×10^{-3})
Integral length scale	Λ_x (m)	57×10^{-3} (57×10^{-3}, 58×10^{-3})
Eddy turnover time	$T_\Lambda(=\Lambda_z/w_{\text{rms}})$ (s)	4.3 (4.3, 4.3)
Kinematic viscosity	ν (m^2 s^{-1})	1.0×10^{-6} (—)
Reynolds number (Taylor)	$Re_\lambda(=w_{\text{rms}}\lambda_z/\nu)$	110 (81, 140)
Reynolds number (integral)	$Re_\Lambda(=w_{\text{rms}}\Lambda_z/\nu)$	760 (750, 760)
Turbulent dissipation rate	$\varepsilon\left(=15\nu\left[w_{\text{rms}}^2/\lambda_z^2\right]\right)$(m^2 s^{-3})	3.8×10^{-5} (1.9×10^{-5}, 5.8×10^{-5})
Kolmogorov length scale	$\eta(=(\nu^3/\varepsilon)^{1/4})$ (m)	0.40×10^{-3} (0.40×10^{-3}, 0.40×10^{-3})
Kolmogorov timescale	$\tau_\eta(=(\nu/\varepsilon)^{1/2}$(s)	0.16 (0.16, 0.17)

into the stirred tank. The particles were near-neutrally buoyant (density $\rho_p = 1007\,\mathrm{kg\,m^{-3}}$) and thus remained mostly suspended during experiments. The characteristic time and length scales of the particle can be compared with the corresponding scales for the fluid-phase turbulence. The particle timescales (τ_p; computed in Appendix A) were 3.64 s for spheres and 5.46 s for ellipsoids, which are close to the turbulent eddy turnover time ($T_\Lambda = 4.3\,\mathrm{s}$). The particle length scales were 8 mm for spheres and between 8 and 16 mm for ellipsoids, which are close to the turbulent Taylor length scale ($\lambda_z = 8.3\,\mathrm{mm}$). The particles' timescales correspond to large turbulent scales, whereas the particles' length scales correspond to small turbulent scales. It was not clear a priori which of these scales would dominate the dynamics, and thus experiments were needed to understand whether particles' timescale or length scale is a better predictor of its rotational statistics in turbulent flow.

[12] It is not trivial to define Reynolds numbers (Re_p) for large particles in a turbulent flow, as discussed in Appendix B, as well as in Bellani and Variano (2012). Appendix B shows that particles' translational motion is outside of the Stokes flow regime, and thus both gravitational settling and turbulent diffusion are expected to influence the transport. Gravitational effects are not negligible for particles of this size, despite the fact that their specific gravity ($\mathrm{SG} = \rho_p/\rho_w = 1.009$, where ρ_w is the density of the fluid) implies near-neutral buoyancy; this dynamic condition might extend to biological particles.

[13] We used hydrogel because of two optical properties: it is refractively matched to water and nearly transparent, which allows passage of a laser light sheet (Byron and Variano 2013). By doing this, we could measure the solid body motion of the particles by imaging embedded optical tracers. We did this via stereoscopic particle image velocimetry (SPIV), in which two cameras and a laser light sheet are used to measure three velocity components at a set of Eulerian locations in a planar region (see Fig. 2). Using the SPIV system (LaVision, Germany), we recorded velocity fields at a data rate of 14.773 Hz. The spatial resolution was 1.38 mm, which was small enough compared with the particle size that we could measure many velocity vectors within each particle. We measured velocity vectors inside the solid particles by tracking clusters of the embedded tracers via standard SPIV.

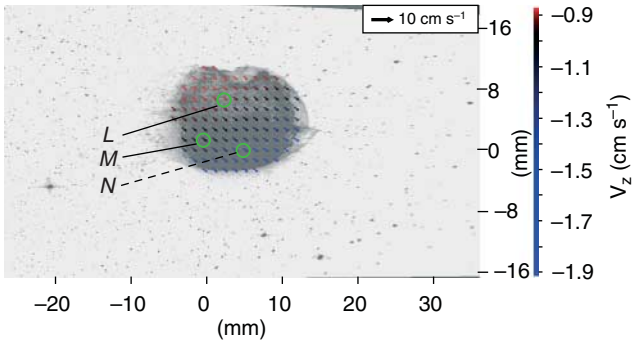

Fig. 2 Stereoscopic particle image velocimetry data superimposed on the particle image from which it was calculated. The dark region in the center is a view of the particle interior, and vectors show the velocity of optical tracers within the particle. Velocity component magnitude is represented by vector size (in *x* and *y*) and vector color (in *z*). Solid body rotation is calculated from Eq. 3.

[14] After collecting three-component velocity measurements along a two-dimensional plane inside each particle, we calculated the particle angular velocity vector, $\mathbf{\Omega} = \Omega_i = [\Omega_x, \Omega_y, \Omega_z]$, using the solid body rotation equation

$$\mathbf{V}_L = \mathbf{V}_M + \mathbf{\Omega} \times \mathbf{R}_{LM}, \tag{3}$$

where $\mathbf{V}_L$ is the velocity vector at any interior point L, $\mathbf{V}_M$ is the velocity vector at a second interior point M, $\mathbf{\Omega}$ is the rotation vector about the center of mass, and $\mathbf{R}_{LM}$ is the distance vector between points L and M. Because we measured three components of velocity at each point (e.g., $\mathbf{V}_L = [V_{Lx}, V_{Ly}, V_{Lz}]$) and all points were coplanar (i.e., $\mathbf{R}_{LM} = [R_{LMx}, R_{LMy}, 0]$), this system of equations was overdetermined in the z-coordinate and underdetermined in the x- and y-coordinates. By including a third interior point (N), all components of $\mathbf{\Omega}$ can be determined. Eq. 3 can be rewritten twice, once in terms of L and N and once in terms of M and N. Using Eq. 3 and the two other permutations, the complete angular velocity vector $\mathbf{\Omega}$ could be determined. This method gives a single value for Ω_x, a single value for Ω_y, and four estimates of Ω_z. We averaged the four estimates of Ω_z, causing our final measurement of Ω_z to contain less measurement noise than the other two components. An ensemble of $\mathbf{\Omega}$ values was determined, one from each possible triplet of vectors V_L, V_N, and V_M. The median

of this ensemble (for each component) was used as the best estimate of particle angular velocity.

[15] We measured $\mathbf{\Omega}$ for a particle as it traveled along its trajectory through the turbulent flow. The trajectories we considered range in length from 8 to 119 SPIV time steps (0.5–8 s in duration). From these we computed the autocovariance for each component $\Omega_i(t)$. The autocovariance of a vector quantity is the second-rank tensor of covariances formed from the components of the vector. For the rotation vector $\Omega_i(t)$, the symmetric autocovariance matrix is

$$R_{\Omega_\alpha\Omega_\beta}(\tau) = \langle \Omega_\alpha(t+\tau)\Omega_\beta(t)\rangle, \quad (4)$$

where α and β subscripts do not imply summation, and expectation value was estimated using an ensemble average across all particle trajectories.

[16] We collected a number of trajectories sufficient to calculate statistically converged values for the first and second moments of the distribution of Ω_i; our data showed convergence for the mean and variance of Ω_i after 300 independent time series. We collected a total of 407 ellipsoid trajectories and 572 sphere trajectories. With these data, we computed a fourth standardized moment (kurtosis) that converged for Ω_z (the low-noise component) but not for the other two components (Ω_x and Ω_y).

Monte Carlo Simulation

[17] Because our data were transformed several times between the raw measurement (tracer locations in a plane) and the final measurement (particle angular velocity vector), it is nontrivial to use error propagation to find the uncertainty (and possible biases) in our measurements. Thus, we used a Monte Carlo simulation to evaluate our measurements of the moments of $\mathbf{\Omega}$. We constructed synthetic angular velocity trajectories using an OU process (Gillespie 1996) and corresponding planar velocity vector fields of the type measured using SPIV. Random noise that is normally distributed with zero mean was added to these vector fields. Both the noisy and noise-free simulated vector fields were passed through the algorithm used to calculate $\mathbf{\Omega}$. By comparing the results from the noise-free and noisy simulated measurements, we assessed the effects of measurement noise on the statistics of $\mathbf{\Omega}$.

Results

[18] Measured autocovariance curves for the spherical and ellipsoidal particles are provided in Fig. 3, A and B, where Eq. 2 is fitted to the data with free parameters α_i^2 and T_{Ω_i}, reported in Table 2. The characteristic timescale (T_{Ω_i}) of exponential decay found in these fits is the Lagrangian integral timescale of particle rotation, and α_i is the noise-free standard deviation of particle angular velocity.

[19] There is a considerable deviation between the data and model at zero lag ($\tau = 0$) in Figs. 3 and 4. We

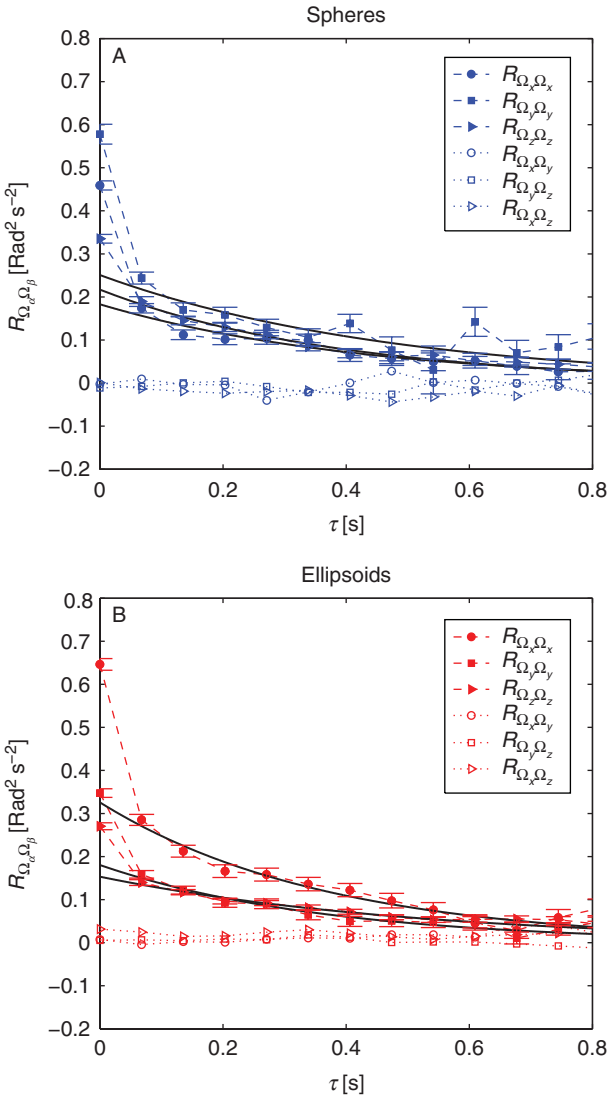

Fig. 3 Autocovariance tensor of particle rotation versus time lag of spherical (A) and ellipsoidal (B) particles. Solid symbols are the diagonal terms of the autocovariance tensor. The error bars are standard error, and the solid line is the exponential fit. Open symbols are the off-diagonal terms of the autocovariance tensor.

Table 2 Parameters and 95% confidence intervals (CIs) from the exponential fit to angular velocity autocovariance: noise-free standard deviation (α_i) and Lagrangian integral timescale (T_{Ω_i}).

Statistic	Spheres (95% CI)	Ellipsoids (95% CI)
α_x (rad s^{-1})	0.43 (0.39, 0.47)	0.57 (0.54, 0.61)
α_y (rad s^{-1})	0.50 (0.40, 0.60)	0.42 (0.39, 0.46)
α_z (rad s^{-1})	0.47 (0.44, 0.49)	0.39 (0.38, 0.41)
T_{Ω_x} (s)	0.43 (0.29, 0.57)	0.37 (0.30, 0.43)
T_{Ω_y} (s)	0.48 (0.15, 0.81)	0.37 (0.28, 0.45)
T_{Ω_z} (s)	0.39 (0.33, 0.45)	0.52 (0.45, 0.59)

attribute this to random noise in the measurement; if this noise is uncorrelated with itself over time, then its signature will be present only in the first point on each curve. This appears to be the case in Figs. 3 and 4, where the data and exponential curve fit agree well away from $\tau = 0$. As a result, the exponential fit parameter α_i can be interpreted as the noise-free variance.

[20] We approximated the magnitude of measurement noise as the difference between the variance measured as the second moment of the angular velocity PDF $\left(\sigma_i^2\right)$ and the noise-free variance measured from the exponential fit to autocovariance $\left(\alpha_i^2\right)$. From these values we defined a signal-to-noise ratio (SNR) as

$$\mathrm{SNR}_i = \sqrt{\frac{\alpha_i^2}{\sigma_i^2 - \alpha_i^2}}. \tag{5}$$

The SNR, measured variance, and noise-free variance are reported in Table 3. The SNR is an essential input to our Monte Carlo analysis; we set the simulated measurement noise in the Monte Carlo simulation so that its SNR matched our measurements. We then used the Monte Carlo results to infer how measurement noise affected the other statistics.

[21] The rotation statistics measured from the particles are provided in Table 3, along with corresponding Monte Carlo results. Because of the isotropy of the turbulence in the tank (see Table 1), the rotation of the particles should also be isotropic. The fitted parameters on the exponential model (Table 2) indicate that this is true, within measurement uncertainty. As expected, the effect of measurement noise was greater for rotation about the x- and y-axes than about the z-axis because Ω_z is the overdetermined component that contains more data. This anisotropic noise effect can be seen in the Monte Carlo results (Table 3): when statistically isotropic rotation was measured with our anisotropic imaging routine, the resulting PDF had anisotropic moments.

[22] Whereas noise-free variance can be calculated as discussed above, no method is available for kurtosis ($\Gamma \equiv \langle a^4 \rangle / \langle a^2 \rangle^2$, where a is a stochastic variable). Thus, we used the Monte Carlo analysis as a guide to understand the kurtosis. The Monte Carlo results show that our measurement method gives kurtosis values that are strongly upward biased. Thus, a distribution of rotation values that is truly Gaussian ($\Gamma = 3$) will appear leptokurtic ($\Gamma > 3$, also known as super-Gaussian) in our measurements. This bias is present in all coordinate directions, though it is stronger in x and y than in z. The biased measurements of kurtosis computed from our experiments are shown in Table 3. Only the z-component is statistically converged; thus, we do not report confidence intervals for the others. The measured values of Γ_z are close to the Monte Carlo predictions for a biased measurement of a Gaussian distribution. In fact, they are slightly smaller than these predictions. We conclude from this that the true distribution of angular velocities in our experiment is near Gaussian and may even be slightly platykurtic ($\Gamma < 3$, also known as sub-Gaussian).

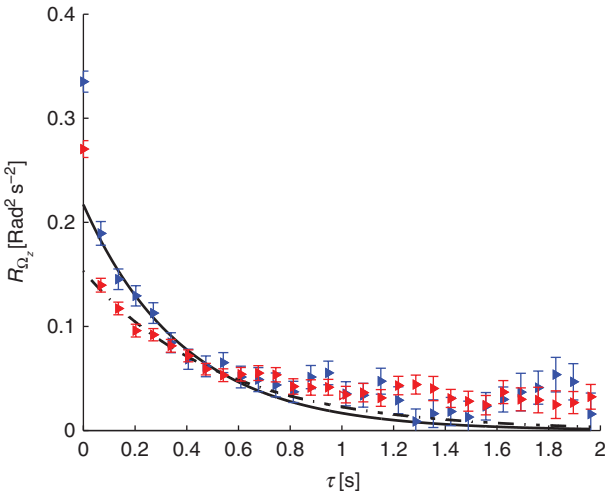

Fig. 4 Autocovariance of particle rotation about the z-axis (Ω_z) for spheres (blue triangles and solid line) and ellipsoids (red triangles and dashed line). Error bars are standard error. Because of a large number of short trajectories, the fit was performed using data for small lag time τ.

Table 3 Moments of angular velocity probability density functions (PDFs) and their Monte Carlo simulation PDFs, with 95% confidence intervals (CIs). Here σ_i is the standard deviation of the PDF of Ω_i and Γ_i is the kurtosis of the PDF of Ω_i. The signal-to-noise ratio (SNR) is calculated by measuring the noise magnitude as the difference between the directly measured standard deviation (σ_i) and the noise-free standard deviation (α_i) obtained from the exponential fit.

	Stereoscopic particle image velocimetry (SPIV)		Monte Carlo simulation	
Statistic	**Spheres (95% CI)**	**Ellipsoids (95% CI)**	**Noise-free (95% CI)**	**Noise included (95% CI)**
SNR_x	0.81 (0.72, 0.91)	1.0 (0.92, 1.1)	—	0.85 (0.89, 0.95)
SNR_y	0.88 (0.66, 1.1)	1.0 (0.92, 1.2)	—	0.87 (0.90, 0.97)
SNR_z	1.4 (1.2, 1.5)	1.1 (1.1, 1.2)	—	1.3 (1.3, 1.4)
$\langle\Omega_x\rangle$ (rad s^{-1})	−0.012 (−0.036, 0.010)	−0.024 (−0.050, −0.00043)	0.033 (0.014, 0.052)	0.018 (−0.014, 0.047)
$\langle\Omega_y\rangle$ (rad s^{-1})	−0.029 (−0.054, 0.0072)	−0.052 (−0.077, −0.032)	0.033 (0.014, 0.052)	0.032 (0.0023, 0.061)
$\langle\Omega_z\rangle$ (rad s^{-1})	0.021 (0.0042, 0.036)	0.011 (−0.0041, 0.025)	0.033 (0.014, 0.052)	0.031 (0.0063, 0.058)
σ_x (rad s^{-1})	0.68 (0.66, 0.69)	0.80 (0.79, 0.82)	1.0 (0.99, 1.0)	1.5 (1.5, 1.5)
σ_y (rad s^{-1})	0.76 (0.73, 0.79)	0.59 (0.57, 0.61)	1.0 (0.99, 1.0)	1.5 (1.4, 1.5)
σ_z (rad s^{-1})	0.58 (0.56, 0.60)	0.52 (0.50, 0.53)	1.0 (0.99, 1.0)	1.3 (1.2, 1.3)
α_x (rad s^{-1})	0.43 (0.39, 0.47)	0.57 (0.54, 0.61)	1.0 (0.99, 1.0)	0.97 (0.94, 1.0)
α_y (rad s^{-1})	0.50 (0.40, 0.60)	0.42 (0.39, 0.46)	1.0 (0.99, 1.0)	0.98 (0.95, 1.0)
α_z (rad s^{-1})	0.47 (0.44, 0.49)	0.39 (0.38, 0.41)	1.0 (0.99, 1.0)	1.01 (0.99, 1.0)
Γ_x	2.7 (—)	2.7 (—)	3.0 (2.9, 3.0)	8.2 (7.3, 9.2)
Γ_y	5.1 (—)	2.9 (—)	3.0 (2.9, 3.0)	7.7 (6.8, 8.7)
Γ_z	5.7 (4.9, 6.7)	5.3 (4.8, 5.9)	3.0 (2.9, 3.0)	6.6 (6.0, 7.2)

Discussion

[23] The hypothesis examined in this study is that the rotation of large particles suspended in turbulence satisfies an Ornstein–Uhlenbeck (OU) process. As mentioned in the introductory remarks, the three characteristics of this stochastic process are exponentially decaying autocovariance, Gaussian distribution, and stationarity. Figs. 3 and 4 show that, other than the noise at zero lag, the exponential decay model is quite effective for particle rotation autocovariance. Based on the discussion of kurtosis above, we conclude that the distribution of angular velocities is likely close to Gaussian. We can assume that the rotation process is stationary whenever the driving flow is stationary. With these three observations as support, we conclude that the OU process is an acceptable model for the Lagrangian angular velocity of large particles.

[24] We can use the OU process to determine the time-dependent rotational eddy diffusivity of large particles in turbulent flow, $K_{\Omega_i}(t)$. In analogy to Eq. 1, this is

$$K_{\Omega_i}(t) = \int_0^t R_{\Omega_i}(\tau)d\tau = \alpha_i^2 T_{\Omega_i}\left(1 - e^{-t/T_{\Omega_i}}\right), \quad (6)$$

from Taylor (1922). This rotational diffusivity allows us to calculate quantities of interest for aquatic organisms, such as the characteristic time for fluid-driven stochastic exploration of orientation space, and the rate at which adjacent organisms lose their relative alignment. Alignment and rotation of organisms at this small scale also impact larger-scale processes; for example, the magnitude of an organism's rotation affects its boundary layer thickness and therefore nutrient uptake, influencing the dynamics of entire communities (Prairie et al. 2012). Fig. 5, A and B, shows the time-varying diffusivity predicted in this way, using α_i^2 and T_{Ω_i} from the exponential fit to our autocovariance measurements (Table 2). When the exponential term diminishes to a negligible value, $K_{\Omega_i}(\tau)$ tends toward a constant value: the Fickian asymptote. The value of the asymptote is calculated as $\hat{K}_{\Omega_i} = \alpha_i^2 T_{\Omega_i}$ and is reported in Table 4.

[25] Our definition of $\boldsymbol{\Omega}$ is the angular velocity vector of a particle about its center of mass, with the three rotation components referenced to a set of coordinate axes that are fixed in the laboratory frame. It would also be possible, though more complicated experimentally, to describe rotation relative to a set of coordinate axes that move with each particle. The two definitions will likely not give identical results, and both would be interesting to know. For example, when studying organisms, the rotation relative to the local axes

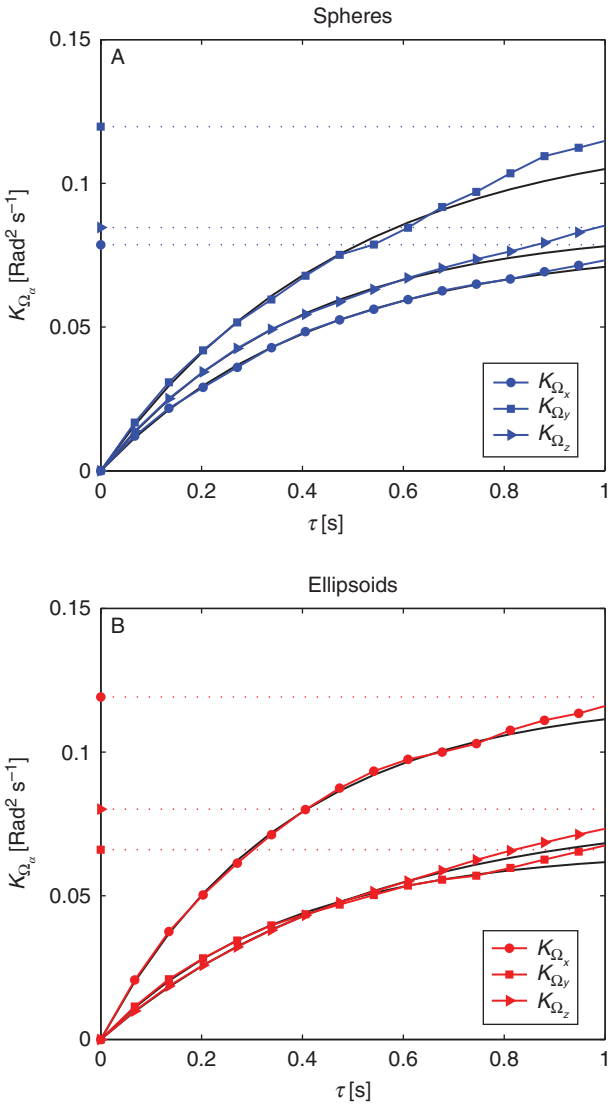

Fig. 5 Time-dependent rotational diffusivity versus time lag for spherical (A) and ellipsoidal (B) particles. Solid lines with symbols are experimental data (noise removed from first point), the black solid line is Eq. 6, and the dotted line is the Fickian asymptote $\hat{K}_{\Omega_\alpha}$ for the respective color symbol.

would directly influence locomotion, while the rotation relative to the laboratory axes would be useful in determining the statistics of the organism's sensory search of three-dimensional space, alignment with other organisms, or alignment with flow features (Berg 1983). Here, we focus only on the rotation relative to the fixed laboratory coordinates and evaluate this rotation while following each particle on its translational random walk. This is the exact meaning of our definition of "Lagrangian angular velocity," and we caution readers to be aware of the other possible definition.

[26] Particle shape appears to have only a minor effect on rotation statistics for the particles considered here. The Lagrangian integral timescales of angular velocity are statistically identical for ellipsoidal and spherical particles (Tables 2 and 4). The variance of angular velocity is also very similar between the two particle shapes, though the statistics are not as conclusive (one component is statistically identical between the two shapes, another is larger for spheres than ellipsoids, and the third is larger for ellipsoids than spheres). Because we examine ensemble statistics rather than individual particle paths (and because we view rotational diffusion as a stochastic process), we are not equipped to investigate specific particle behaviors such as Jefferey (1922) orbits. Furthermore, our particles are tumbling in a high Reynolds number turbulent flow (out of the Stokes regime) and therefore are not analogous to Jefferey's (1922) theory, as previously stated. For the same reason, the model of a sphere in creeping flow would not be appropriate here (Kiørboe and Visser 1999; Catton et al. 2012).

[27] From our experiments, since particle shape appears to have little influence on rotation statistics, we conclude that particle rotation dynamics are dominated by the large scales of fluid motion. This is consistent with the results of Nguyen et al. (2011), who found that the diatoms with spines all rotate with a statistically identical period, regardless of the number of spines. In our experiment, the ellipsoids and spheres will likely interact with the fluid differently on small scales (i.e., the scale of particle diameter and Taylor length scale), because of their shapes and related wake effects. However, these differences appear to be of minor importance in determining the particle rotation. The large scales of turbulent motion appear to have the largest effect on particle rotation. From this conclusion, we can infer that particles' Stokesian relaxation timescale, the characteristic response time delay for a particle in Stokes flow, is a more appropriate predictor of dynamics than the particle size scale. The reasoning is as follows. The Stokesian relaxation timescale of particles considered here is nearly equal to the eddy turnover time. This implies that small-scale turbulent features will not persist long enough to elicit a response from the particles, and

Table 4 Calculation of rotational diffusivity, $\hat{K}_{\Omega_i}$. Comparison of the laboratory measurements and Monte Carlo simulations shows that measurement noise has only a slight effect on the calculation of the rotational diffusivity.

	Stereoscopic particle image velocimetry (SPIV)		Monte Carlo simulation	
Statistic	**Spheres (95% CI)**	**Ellipsoids (95% CI)**	**Noise-free (95% CI)**	**Noise included (95% CI)**
α_x (rad s^{-1})	0.43 (0.39, 0.47)	0.57 (0.54, 0.61)	1.0 (0.99, 1.0)	0.97 (0.94, 1.0)
α_y (rad s^{-1})	0.50 (0.40, 0.60)	0.42 (0.39, 0.46)	1.0 (0.99, 1.0)	0.98 (0.95, 1.0)
α_z (rad s^{-1})	0.47 (0.44, 0.49)	0.39 (0.38, 0.41)	1.0 (0.99, 1.0)	1.01 (0.99, 1.0)
T_{Ω_x} (s)	0.43 (0.29, 0.57)	0.37 (0.30, 0.43)	0.13 (0.13, 0.14)	0.13 (0.12, 0.14)
T_{Ω_y} (s)	0.48 (0.15, 0.81)	0.37 (0.28, 0.45)	0.13 (0.13, 0.14)	0.13 (0.12, 0.14)
T_{Ω_z} (s)	0.39 (0.33, 0.45)	0.52 (0.45, 0.59)	0.13 (0.13, 0.14)	0.13 (0.12, 0.14)
$\hat{K}_{\Omega_x}$ (rad^2 s^{-1})	0.079 (0.048, 0.11)	0.12 (0.093, 0.15)	0.14 (0.13, 0.15)	0.12 (0.11, 0.13)
$\hat{K}_{\Omega y}$ (rad^2 s^{-1})	0.12 (0.025, 0.21)	0.066 (0.048, 0.084)	0.14 (0.13, 0.15)	0.12 (0.11, 0.13)
$\hat{K}_{\Omega_z}$ (rad^2 s^{-1})	0.086 (0.069, 0.10)	0.080 (0.068, 0.092)	0.14 (0.13, 0.15)	0.13 (0.12, 0.14)

thus only large-scale motions will matter in determining particle dynamics.

[28] The idea that particle rotation is governed by a relatively large timescale has many implications for behavioral models of the larger plankton, such as the prey-capture model for larval fish presented in MacKenzie et al. (1994). In these and similar cases (e.g., Dower et al. 1997), the persistence timescale of rotation can be compared with model parameters such as the minimum pursuit time to determine if rotation should be included in the model. Our observation of shape-independent rotation suggests that this persistence timescale can be estimated with the Stokes relaxation time and that this approach is a more accurate predictor of particle dynamics than one based on length scales. Similar to our results for rotation, dominance of large-scale fluid motion in determining particle translation is discussed in Komasawa et al. (1974). In contrast, the particle size scale, being similar to the Taylor length scale, implies that motions significantly smaller than the energy containing scales could matter in determining particle dynamics.

[29] The stochastic behavior of particle rotation appears to be inherited directly from the large scales of surrounding turbulence, and thus we expect that particle rotation will scale with the energy-containing motions of turbulence. This conceptual model suggests that angular velocity variance will scale with the turbulent kinetic energy E_k, and scale inversely with the square of the turbulent integral length scale Λ, as

$$\alpha_i^2 \sim E_k \Lambda^{-2}. \tag{7}$$

We also predict that the Lagrangian timescale of rotation T_{Ω_i} should follow the same scaling as the Lagrangian timescale of translation T_L; that is,

$$T_{\Omega_i} \sim T_L \sim E_k \varepsilon^{-1}, \tag{8}$$

where ε is the turbulent kinetic energy dissipation rate (Pope 2000). Together, these results suggest that the rotational diffusivity $\hat{K}_{\Omega_i} = \alpha_i^2 T_{\Omega_i}$ will scale as $\hat{K}_{\Omega_i} \sim E_k^2 \Lambda^{-2} \varepsilon^{-1}$. Using the scaling relationship $\varepsilon \sim E_k^{3/2} \Lambda^{-1}$, we can rewrite our result as

$$\hat{K}_{\Omega_i} \sim E_k^{1/2} \Lambda^{-1}. \tag{9}$$

A heuristic description of this scaling can be made in two parts. First, larger turbulent kinetic energy corresponds to larger rotational diffusion. Second, at a fixed turbulent kinetic energy, particles will undergo the most rotational diffusion when the integral scale is as small as possible. This makes sense because minimizing the integral scale at constant E_k maximizes fluid enstrophy. We can write the scaling law as $\hat{K}_{\Omega_i} = C E_k^{1/2} \Lambda^{-1}$ and use the measurements in this study to approximate the constant $C \approx 0.5$. This result should be used with caution because the measurements from which C is approximated cover only one point in parameter space. Furthermore, these results should be applied only to particles sharing dynamical properties similar to those considered here.

[30] For spherical and ellipsoidal particles suspended in homogeneous, isotropic turbulence, we have shown that the particle angular velocity can be modeled as an OU process. This conclusion follows from our laboratory measurements showing that the Lagrangian

autocovariance of particles' angular velocity decays exponentially (Fig. 3). Our measurements also show that the particle rotation PDF is close to Gaussian, a conclusion that requires the use of a Monte Carlo simulation to evaluate the propagation of measurement noise through our analysis. Comparing particles of two different shapes, we found that the greater eccentricity of the ellipsoid does not strongly influence its rotational diffusion. Both ellipsoids and spheres exhibit similar integral timescales of rotation and angular velocity variances, from which we infer that particle rotation is governed by large turbulent scales.

Significance to Aquatic Environments

[31] Our results can be used to understand organisms with physical characteristics similar to the particles studied here, specifically organisms that are nonspherical, nearly neutrally buoyant, and within the size range of the turbulent inertial subrange. Depending on the organism and the ambient turbulence, these can include copepods, diatom chains, and larvae. A good size match for our particles is the larvae of most teleost fishes (Osse et al. 1997). The distribution of linear and angular velocities that these larvae experience is central to their survival, affecting feeding, recruitment, and predator avoidance (Grünbaum and Strathmann 2003; Peng and Dabiri 2009).

[32] One application of our results is to quantify how turbulent rotation dictates the timescales over which an organism samples orientation space. Any sensory organs that the organism uses must be swept across space, unless they are omnidirectional. This sweeping may be driven by organism locomotion only, by turbulent rotational diffusion only, or by a combination of both. For the flow-particle combination studied here, particles exploring space by turbulent rotational diffusion only will complete one entire rotation cycle via diffusion in an average of roughly 6 min ($T_{2\pi} = (2\pi)^2/\hat{K}_{\Omega_i} \approx 360$ s). A similar approach can be used to quantify the breakdown of alignment within groups of organisms. If we consider that mutual alignment is lost after the average individual diffusively rotates over an angle of $\pi/8$, then for the particles considered here, alignment is lost after 1.5 s.

[33] For particles of sizes different from those used in the models here, approximate results for rotational diffusivity can be obtained provided that the particles are in the same dynamical regime as studied here. In this regime, the relative motion between fluid and particle is outside the creeping flow regime ($Re_p > 1$), the Stokesian relaxation timescale is similar to the large eddy turnover time, and the particle length scale is within the inertial subrange. For such particles, our analysis suggests that the rotational diffusivity scales as $\hat{K}_{\Omega_i} \sim E_k^{1/2}\Lambda^{-1}$.

[34] Our results show the timescales of rotation to be comparable to the large timescales of the ambient turbulence, which is significant because it gives some predictive power. Knowledge of this "forgetting timescale" is crucial for the study of alignment in aquatic organisms because it may impact such behaviors as chain formation or schooling (Pahlow et al. 1997; Grünbaum 1998). This result, as well as the others presented herein, can be helpful in evaluating the interplay between passive and active locomotion by organisms. That is, it is an open question to what degree an organism's rotation is caused by its own actions versus hydrodynamic forcing. Understanding this can help shed light on rotation-governed behaviors such as the run-and-tumble approach to chemotaxis (Adler and Tso 1974; Tailleur and Cates 2008).

[35] Our results on shape are of value to researchers investigating how the shape of an organism affects its interactions with its environment (Tytell et al. 2010; Marcos et al. 2012; Peng and Alben 2012). The results of this study indicate that in our size range, ellipsoid eccentricity between 1 and 2 has no significant effect on angular velocity variance or integral timescale. This observation, plus our explanation for why this is the case, can be useful for a subset of conditions found in nature.

[36] Microautonomous underwater vehicles (μAUVs) may be used as part of future work to measure and monitor aquatic environments. The results given here can aid in the design of these vehicles. For example, direction-finding is strongly dependent on orientation, requiring complex control systems to maintain the original heading of the vehicle (Cox and Wei 1995; Yun et al. 1999). Thus, being able to predict the influence of tur-

bulent flow on μAUV rotation may streamline and simplify such control systems.

Acknowledgments We thank Gabriele Bellani for support in the laboratory measurements and analyses, Matt Ritter and Audric Collignon for early development of the measurement technique, and Jason Lepore, Matt Ford, and Yoram Rubin for insightful discussions. C.R.M.'s participation was conducted through undergraduate course work supported by the Department of Civil and Environmental Engineering at the University of California, Berkeley. M.L.B.'s participation was supported by Center for Integrative Biomechanics in Education and Research through National Science Foundation Integrative Graduate Education and Research Traineeship 0903711.

Appendix A

[A1] The Stokesian relaxation time can be used to approximate the timescale with which particles will respond to fluid motions in the turbulent field. This scale is $\tau_p \equiv \rho_p d_p^2/18\rho_f \nu$, which is derived using a simpler flow than considered here. Specifically, this definition of τ_p is the exponential timescale with which spherical particles in creeping flow approach their terminal velocity in a uniform steady flow. Calculating this timescale for the spheres, $\tau_{p,s} = 3.64$ s.

[A2] To estimate the response behavior of ellipsoids, one can consider the average relaxation timescale of randomly oriented ellipsoidal particles in creeping flow. Zhang et al. (2001) derived this timescale in terms of ellipsoid eccentricity ℓ and the relaxation time of a sphere whose diameter equals the ellipsoid's minor axis $\tau_{p,q}$ as

$$\tau_{p,e} = \tau_{p,q}\ \ell \frac{log(\ell + \sqrt{\ell^2 - 1})}{\sqrt{\ell^2 - 1}}. \qquad \text{(S1)}$$

[A3] In our study, $\ell = 2$, and the equivalent sphere is equal to the sphere considered above ($\tau_{p,q} = \tau_{p,s}$). Thus, the ellipsoid relaxation timescale is $\tau_{p,e} = 1.5\tau_{p,s} = 5.46$ s. It is worth emphasizing that the particles in this study are likely not experiencing creeping flow, and thus the timescales are not explicit predictions but, rather, serve as scales to guide the interpretation of results.

Appendix B

[B1] The traditional definition of particle Reynolds number is $Re_p \equiv Wd/\nu$, where d is particle diameter and W is the relative velocity between the particle center-of-mass velocity V and fluid velocity far from the particle wake U. In a quiescent fluid, we use the Clift and Gauvin (1970) expression for drag on a sphere to predict a terminal velocity of 3.6 cm s^{-1} and corresponding $Re_p = 255$ for spheres having specific gravity of 1.009 and diameter of 8 mm. To the authors' knowledge, there is no drag model for prolate ellipsoids that gives the expected settling velocity in quiescent fluid for particles at a random orientation. However, most related work suggests that the drag coefficient will be order 1, and the relevant length scale will be between the major and minor axis lengths. With these approximations, the Reynolds number for the ellipsoids will be similar to that found for spheres ($Re_p = 255$, shown above).

[B2] The above results may not accurately describe the particle motion measured herein because the fluid flow is far from quiescent. Turbulent fluctuating velocities in the fluid phase prevent a straightforward definition of the relative velocity W, for lack of a single dynamically relevant velocity U. If an expectation velocity ($\langle U \rangle$) is used to quantify the fluid phase, one obtains an unsteady relative velocity $W_1 \equiv \langle U \rangle - V$, and by taking the expectation value of W_1, one obtains the stochastically steady relative velocity $W_2 \equiv \langle U \rangle - \langle V \rangle$. There is no empirical model allowing the prediction of $\langle V \rangle$ for either spheres or ellipsoids. But we estimate W_2 roughly by equating the weight of a particle to an ensemble average drag force $F_D \equiv \frac{1}{2}\rho C_D a W_2^2$, where a is the cross-sectional area. By assuming that the drag coefficient is bounded by 0.1 and 10, this estimate suggests that Re_p is above 70 and below 7000, for both spheres and ellipsoids.

[B3] When fluctuating velocities exceed expectation velocities, then it may be more appropriate to define particle Reynolds number from a fluctuating velocity. A practical option is

$$W_3 \equiv \sqrt{(U - \langle U \rangle)^2} - \sqrt{(V - \langle V \rangle)^2}. \qquad \text{(S2)}$$

It is appealing to define $W_4 \equiv \sqrt{(U-V)^2}$, but this incurs the challenge of defining U, as discussed above. Bellani and Variano (2012) measured W_3 for the particles measured in this study, in a very similar turbulent flow, and found that Re_p was 46 for spheres and 79 for ellipsoids.

[B4] With the above results, it is possible to conclude that particle motions examined here respond both to gravitational settling and to the drag response to turbulent velocity fluctuations in the fluid phase. Furthermore, in both cases, particles move in such a manner that the fluid-particle interaction is outside the regime defined as creeping flow.

References

Adler, J., and W.-W. Tso. 1974. Decision-making in bacteria: Chemotactic response of *Escherichia coli* to conflicting stimuli. Science. **184**: 1292–1294. doi:10.1126/science.184.4143.1292.

Bagchi, P., and S. Balachandar. 2002. Effect of free rotation on the motion of a solid sphere in linear shear flow at moderate *Re*. Phys. Fluids. **14**: 2719–2737. doi:10.1063/1.1487378.

Batchelor, G. K. 1967. An Introduction to Fluid Dynamics. Cambridge University Press.

Bellani, G., M. L. Byron, A. G. Collignon, C. R. Meyer, and E. A. Variano. 2012. Shape effects on turbulent modulation by large nearly neutrally buoyant particles. J. Fluid Mech. **712**: 41–97. doi:10.1017/jfm.2012.393.

Bellani, G., and E. A. Variano. 2012. Slip velocity and drag of large neutrally buoyant particles in turbulent flows. New J. Phys. **14**: 125009, doi:10.1088/1367-2630/14/12/125009.

Berg, H. C. 1983. Random Walks in Biology. Princeton Univ. Press.

Byron, M. L., and E. A. Variano. 2013. Refractive-index-matched hydrogel materials for measuring flow-structure interactions. Exp. Fluids. **54**: 1456, doi:10.1007/s00348-013-1456-z.

Čada, G. F. 1997. Shaken not stirred—the recipe for a fish-friendly turbine. Proc. Water Power. **97**: 1–9.

Catton, K. B., D. R. Webster, and J. Yen. 2012. The effect of fluid viscosity, habitat temperature, and body size on the flow disturbance of *Euchaeta*. Limnol. Oceanogr. Fluids Environ. **2**: 80–92. doi:10.1215/21573689-1894514.

Clift, R., and H. W. Gauvin. 1970. The motion of particles turbulent gas streams. Proc. Chemeca. **1**: 14–28.

Clift, R., J. R. Grace, and M. E. Weber. 2005. Bubbles, Drops, and Particles. Dover.

Cox, R., and S. Wei. 1995. Advances in the state of the art for AUV inertial sensors and navigation systems. IEEE J. Oceanic Eng. **20**: 361–366. doi:10.1109/48.468253.

Doob, J. L. 1942. The Brownian movement and stochastic equations. Ann. Math. **43**: 351–369. doi:10.2307/1968873. Pp. 319–337. Reprinted in N. Wax [ed.], *Selected Papers on Noise and Stochastic Processes*. Dover, 1954.

Dower, J. F., T. J. Miller, and W. C. Leggett. 1997. The role of microscale turbulence in the feeding ecology of larval fish. Adv. Mar. Biol. **31**: 169–220. doi:10.1016/S0065-2881(08)60223-0.

Durham, W. M., J. O. Kessler, and R. Stocker. 2009. Disruption of vertical motility by shear triggers formation of thin phytoplankton layers. Science. **323**: 1067–1070. doi:10.1126/science.1167334.

Fischer, H. B., J. E. List, C. R. Koh, J. Imberger, and N. H. Brooks. 1979. Mixing in Inland and Coastal Waters. Academic Press.

Giacobello, M., A. Ooi, and S. Balachandar. 2009. Wake structure of a transversely rotating sphere at moderate Reynolds numbers. J. Fluid Mech. **621**: 103–130. doi:10.1017/S0022112008004655.

Gillespie, D. T. 1996. Exact numerical simulation of the Ornstein-Uhlenbeck process and its integral. Phys. Rev. E Stat. Phys. Plasmas Fluids Relat. Interdiscip. Topics. **54**: 2084–2091. doi:10.1103/PhysRevE.54.2084.

Grünbaum, D. 1998. Schooling as a strategy for taxis in a noisy environment. Evol. Ecol. **12**: 503–522. doi:10.1023/A:1006574607845.

Grünbaum, D., and R. R. Strathmann. 2003. Form, performance and trade-offs in swimming and stability of armed larvae. J. Mar. Res. **61**: 659–691. doi:10.1357/002224003771815990.

Jefferey, G. B. 1922. The motion of ellipsoidal particles immersed in a viscous fluid. Proc. Roy. Soc. Lond. Ser. A. **102**: 161–179. doi:10.1098/rspa.1922.0078.

Jenny, M., J. Dušek, and G. Bouchet. 2004. Instabilities and transition of a sphere falling or ascending freely in a Newtonian fluid. J. Fluid Mech. **508**: 201–239. doi:10.1017/S0022112004009164.

Kiørboe, T., and A. W. Visser. 1999. Predator and prey perception in copepods due to hydromechanical signals. Mar. Ecol. Prog. Ser. **179**: 81–95. doi:10.3354/meps179081.

Koch, D. L., and E. S. G. Shaqfeh. 1989. The instability of a dispersion of sedimenting spheroids. J. Fluid Mech. **209**: 521–542. doi:10.1017/S0022112089003204.

Komasawa, I., R. Kuboi, and T. Otake. 1974. Fluid and particle motion in turbulent dispersion—I: Measurement of turbulence of liquid by continual pursuit of tracer particle motion. Chem. Eng. Sci. **29**: 641–650. doi:10.1016/0009-2509(74)80178-8.

Machemer, H., and R. Bräucker. 1992. Gravireception and graviresponses in ciliates. Acta Protozool. **31**: 185–214.

MacKenzie, B. R., T. J. Miller, S. Cyr, and W. C. Leggett. 1994. Evidence for a dome-shaped relationship between turbulence and larval fish ingestion rates. Limnol. Oceanogr. **39**: 1790–1799. doi:10.4319/lo.1994.39.8.1790.

Marcos, H. C., Fu, T. R. Powers, and R. Stocker. 2012. Bacterial rheotaxis. Proc. Natl. Acad. Sci. USA. **109**: 4780–4785. doi:10.1073/pnas.1120955109.

Mortensen, P. H., H. I. Andersson, J. J. J. Gillissen, and B. J. Boersma. 2007. Particle spin in a turbulent shear flow. Phys. Fluids. **19**: 078109, doi:10.1063/1.2750677.

Mortensen, P. H., H. I. Andersson, J. J. J. Gillissen, and B. J. Boersma. 2008a. Dynamics of prolate ellipsoidal particles in a turbulent channel flow. Phys. Fluids. **20**: 093302, doi:10.1063/1.2975209.

Mortensen, P. H., H. I. Andersson, J. J. J. Gillissen, and B. J. Boersma. 2008b. On the orientation of ellipsoidal particles in a turbulent shear flow. Int. J. Multiphase Flow. **34**: 678–683. doi:10.1016/j.ijmultiphaseflow.2007.12.007.

Naso, A., and A. Prosperetti. 2010. The interaction between a solid particle and a turbulent flow. New J. Phys. **12**: 033040, doi:10.1088/1367-2630/12/3/033040.

Nguyen, H., L. Karp-Boss, P. A. Jumars, and L. Fauci. 2011. Hydrodynamic effects of spines: A different spin. Limnol. Oceanogr. Fluids Environ. **1**: 110–119. doi:10.1215/21573698-1303444.

Osse, J. W. M., J. G. M. van den Boogaart, G. M. J. van Snik, and L. van der Sluys. 1997. Priorities during early growth of fish larvae. Aquaculture. **155**: 249–258. doi:10.1016/S0044-8486(97)00126-9.

Pahlow, M., U. Riebesell, and D. A. Wolf-Gladrow. 1997. Impact of cell shape and chain formation on nutrient acquisition by marine diatoms. Limnol. Oceanogr. **42**: 1660–1672. doi:10.4319/lo.1997.42.8.1660.

Peng, J., and S. Alben. 2012. Effects of shape and stroke parameters on the propulsion performance of an axisymmetric swimmer. Bioinspir. Biomim. **7**: 016012, doi:10.1088/1748-3182/7/1/016012.

Peng, J., and J. O. Dabiri. 2009. Transport of inertial particles by Lagrangian coherent structures: Application to predator-prey interaction in jellyfish feeding. J. Fluid Mech. **623**: 75–84. doi:10.1017/S0022112008005089.

Pope, S. B. 2000. Turbulent Flows. Cambridge Univ. Press, doi:10.1017/CBO9780511840531.

Prairie, J. C., K. R. Sutherland, K. J. Nickols, and A. M. Kaltenberg. 2012. Biophysical interactions in the plankton: A cross-scale review. Limnol. Oceanogr. Fluids Environ. **2**: 121–145. doi:10.1215/21573689-1964713.

Reidenbach, M. A., J. R. Koseff, and M. A. R. Koehl. 2009. Hydrodynamic forces on larvae affect their settlement on coral reefs in turbulent, wave-driven flow. Limnol. Oceanogr. **54**: 318–330. doi:10.4319/lo.2009.54.1.0318.

Richardson, L. F. 1926. Atmospheric diffusion shown on a distance-neighbour graph. Proc. R. Soc. Lond. Ser. A. **110**: 709–737. doi:10.1098/rspa.1926.0043.

Roberts, A. M., and F. M. Deacon. 2002. Gravitaxis in motile microorganisms: The role of fore-aft body asymmetry. J. Fluid Mech. **452**: 405–423. doi:10.1017/S0022112001006772.

Rybalko, M., E. Loth, and D. Lankford. 2012. A Lagrangian particle random walk model for hybrid RANS/LES turbulent flows. Powder Technol. **221**: 105–113. doi:10.1016/j.powtec.2011.12.042.

Shin, M., and D. L. Koch. 2005. Rotational and translational dispersion of fibres in isotropic turbulent flows. J. Fluid Mech. **540**: 143–173. doi:10.1017/S0022112005005690.

Tailleur, J., and M. E. Cates. 2008. Statistical mechanics of interacting run-and-tumble bacteria. Phys. Rev. Lett. **100**: 218103, doi:10.1103/PhysRevLett.100.218103.

Taylor, G. I. 1922. Diffusion by continuous movements. Proc. London Math. Soc. Ser. A. **s2-20**: 196–212. doi:10.1112/plms/s2-20.1.196.

Taylor, G. I. 1953. Dispersion of soluble matter in solvent flowing slowly through a tube. Proc. R. Soc. Lond. Ser. A. **219**: 186–203. doi:10.1098/rspa.1953.0139.

Tritico, H. M., and A. J. Cotel. 2010. The effects of turbulent eddies on the stability and critical swimming speed of creek chub (*Semotilus atromaculatus*). J. Exp. Biol. **213**: 2284–2293. doi:10.1242/jeb.041806.

Tytell, E. D., I. Borazjani, F. Sotiropoulos, T. V. Baker, E. J. Anderson, and G. V. Lauder. 2010. Disentangling the functional roles of morphology and motion in the swimming of fish. Integr. Comp. Biol. **50**: 1140–1154. doi:10.1093/icb/icq057.

Variano, E. A., and E. A. Cowen. 2008. A random-jet-stirred turbulence tank. J. Fluid Mech. **604**: 1–32. doi:10.1017/S0022112008000645.

Visser, A. W. 2001. Hydromechanical signals in the plankton. Mar. Ecol. Prog. Ser. **222**: 1–24. doi:10.3354/meps222001.

Visser, A. W., and T. Kiørboe. 2006. Plankton motility patterns and encounter rates. Oecologia. **148**: 538–546. doi:10.1007/s00442-006-0385-4.

Webb, P. W., and A. J. Cotel. 2010. Turbulence: Does vorticity affect the structure and shape of body and fin propulsors? Integr. Comp. Biol. **50**: 1155–1166. doi:10.1093/icb/icq020.

Yamazaki, H., and K. D. Squires. 1996. Comparison of ocean turbulence and copepod swimming. Mar. Ecol. Prog. Ser. **144**: 299–301. doi:10.3354/meps144299.

Yun, X., E. R. Bachmann, R. B. McGhee, R. H. Whalen, R. L. Roberts, R. G. Knapp, A. J. Healey, and M. J. Zyda. 1999. Testing and evaluation of an integrated GPS/INS system for small AUV navigation. IEEE J. Oceanic Eng. **24**: 396–404. doi:10.1109/48.775301.

Zhang, H., G. Ahmadi, F. Fan, and J. McLaughlin. 2001. Ellipsoidal particles transport and deposition in turbulent channel flows. Int. J. Multiphase Flow. **27**: 971–1009. doi:10.1016/S0301-9322(00)00064-1.

Received: 10 October 2012
Amended: 01 February 2013
Accepted: 15 March 2013